

Sustainable Energy & Fuels

Screening Transition Metal Electrodes for Achieving near 100% Selectivity to Urea via Electroreduction of NO3- and CO2 at 100 mA/cm2 Current Density

Journal:	Sustainable Energy & Fuels
Manuscript ID	SE-ART-06-2024-000841.R2
Article Type:	Paper
Date Submitted by the Author:	06-Oct-2024
Complete List of Authors:	Kani, Nishithan; Technical University of Denmark Goyal, Ishita; University of Illinois at Chicago, Chemical Engineering Olusegun, Samuel; Texas Tech University System Chinnabattigalla, Sreenivasulu; University of Illinois Chicago, Department of Chemistry Bhawnani, Rajan; University of Illinois at Chicago, Chemical Engineering Glusac, Ksenija; University of Illinois at Chicago, Chemistry; Argonne National Labratory, Chemical Science and Engineering Gauthier, Joseph; Texas Tech University, Department of Chemical Engineering Singh, Meenesh; University of Illinois Chicago, Department of Chemical Engineering

SCHOLARONE™ Manuscripts

Screening Transition Metal Electrodes for Achieving near 100% Selectivity to Urea via Electroreduction of NO₃⁻ and CO₂ at 100 mA/cm² Current Density

Nishithan C. Kani^{a#}, Ishita Goyal^{a#}, Samuel Olusegun^b, Sreenivasulu Chinnabattigalla^c, Rajan R. Bhawnani^a, Ksenija D. Glusac^{c, d}, Joseph A. Gauthier^{b*}, and Meenesh R. Singh^{a*}

- ^a Department of Chemical Engineering, University of Illinois Chicago, Chicago, IL 60607, United States.
- ^b Department of Chemical Engineering, Texas Tech University, Lubbock, TX 79409, United States
- ^c Department of Chemistry, University of Illinois Chicago, Chicago, IL 60607, United States
- ^dChemical Sciences and Engineering Division, Argonne National Laboratory, Lemont, Illinois 60439, United States.

Authors contributed equally

* Corresponding Authors

Corresponding Authors:

Prof. Meenesh R. Singh, Email: mrsingh@uic.edu

Prof. Joseph A. Gauthier, Email: Joe.Gauthier@ttu.edu

Keywords: Electrochemical urea synthesis, Electrochemical nitrate reduction, Electrochemical CO₂ reduction, Nitrate removal, Electrochemical C-N coupling.

Abstract

The current method to synthesize urea is highly energy-intensive and has a massive carbon footprint. Electrochemical synthesis of urea from NO_3^- and CO_2 is an attractive and sustainable way as renewable energy can be used to synthesize green urea at ambient conditions by utilizing the waste NO_3^- and CO_2 from the air or flue gas. In this work, we conduct a thorough catalytic screening of various metal-based catalysts. ~100 % urea Faradaic efficiency and ~-100 mA/cm² of urea current density is observed at -1.2 V vs. RHE when Ag GDE is used as a working electrode. FTIR analysis further confirms the formation of urea and the presence of *CO intermediates. The excellent kinetics and selectivity towards urea on Ag are explained by a combination of facile first and second C-N bond formation steps and an endergonic ($\Delta G > 1.5 \text{ eV}$) formamide (HCONH₂) formation step from *CONH₂ from our DFT studies.

Introduction

Urea is one of the major nitrogenous fertilizers (70 %) and the primary source of nitrogen supply for the plants.^{1, 2} Apart from fertilizers, urea is used for the synthesis of resins such as melamine, and urea-formaldehyde resin³, and as a diesel exhaust fluid that is used in diesel engines for selective catalytic reduction of NOx.4, 5 Urea is synthesized industrially by the Bosch-Meiser process that involves the conversion of CO₂ and NH₃ at a high pressure of 110 atm and elevated temperatures between 160 - 180 °C.6 NH₃, a primary raw material for urea production, is manufactured by the Haber-Bosch process at high temperatures (400 - 500 °C) and high pressures (100 – 200 atm) utilizing H2 from the steam reforming process. 48 % of the global NH₃ produced is used for urea manufacturing and the overall process to make urea is highly energyintensive and has a massive carbon footprint.8 It is desired that urea manufacturing be decarbonized by synthesizing urea using renewable energy and readily available feedstocks via an electrochemical approach. Electrochemical synthesis of urea from N₂ to CO₂ is very attractive, but the process is very challenging due to the stable N≡N (941 kJ/mol) and lower solubility of N₂ in an agueous medium.^{9, 10} On the other hand, N=O has lower bond dissociation energy (204 kJ/mol) in comparison with N≡N (941 kJ/mol)⁹ and hence it is less challenging to activate NO₃⁻ in comparison to N₂. ¹¹ Industrially, NO₃ is manufactured from NH₃, and electrochemical conversion NO₃⁻ to NH₃ would make sense only in the context of recycling the waste NO₃⁻. ^{12, 13} Synthesizing urea from the NO₃- and CO₂ has a major environmental impact than utilizing NH₃ and CO₂ as the existing process involves 21 to 29 billion gigajoules of energy globally per year and 0.7 to 2.3 tons of CO₂ emissions per ton equivalent of urea produced.¹⁴

NO₃⁻ is a major source of pollutants in agricultural run-off water, industrial processing plants, and ammunition waste.¹⁵ ANSOL (65 % Ammonium nitrate solution) is a major waste stream produced by Holstan army ammunition plant at a rate of 10 million pounds per year. ANSOL is extremely hazardous, and unsafe to store, and utilization of ANSOL in value-added products is one of the problems posed by the Strategic Environmental Research and Development Program (SERDP) of the US Department of Defense. ANSOL is usually sold to mining industries, but there is an inconsistent demand, and the existing methods involve thermal degradation of ANSOL, which is inefficient and not environmentally friendly. NH₃ can be recovered from ANSOL by stripping after shifting the pH of the solution towards the alkaline side. This results in a large concentration of NO₃- stream that is environmentally hazardous and needs to be treated.

In this study, we focus on co-reducing NO_3^- and CO_2 electrochemically to synthesize urea. Direct electrochemical co-reduction of NO_3^- and CO_2 is attractive as green urea can be produced in a decentralized manner with lower capital costs. Also, this study would help us provide insights into the electrochemical C-N coupling, which has not been explored extensively in the literature. Understanding electrochemical C-N coupling would enable selective synthesis of chemicals such as urea, methyl amine, acetamide, and benzamide, which are used as a precursor in the synthesis of several commercial drugs such as analgesics, antiemetics, antipsychotics, etc. The objective of the current study is a selective electrochemical synthesis of urea from NO_3^- and CO_2 .

Electrochemical CO₂ reduction reactions (CO₂RR) have been thoroughly investigated in the literature. ¹⁶ Cu is the only catalyst for producing C₂ products like C₂H₄. ¹⁷ Ag¹⁸, Au¹⁹, and Zn²⁰ are prominent catalysts to produce CO. Electrochemical NO₃- reduction to NH₃ (NRN) has been investigated on a wide variety of catalysts, including Cu^{21, 22}, Pd²³, Fe²⁴, Ti¹⁵, and Co^{25, 26} etc., and among them, Cobalt has demonstrated good activity for the electrochemical synthesis of NH₃ from NO₃⁻ in alkaline media.^{25, 26} Moreover, Ru-based catalysts²⁷ have shown high efficiency in NH₃ synthesis from NO₃-, enabling the reaction at much more positive potentials, around 0 V vs. RHE. While cobalt can effectively promote the conversion of nitrate to nitrite at relatively positive potentials, it is less efficient for deeper nitrate reduction, which requires potentials well below 0 V vs. RHE. Early works of Shibata et al. ²⁸⁻³² report the electrochemical reduction of NO₂-/NO₃ and CO₂ on various transition metal-based gas diffusion electrodes. Zn exhibited the highest urea current efficiency of 35 % at -1.75 V vs. SHE from the electrochemical reduction of NO₃⁻ and CO₂. They proposed from experimental evidence that NH₃-like precursor formed from NO₂- and COlike precursor is essential for urea synthesis. However, their works do not clearly state several things, such as the experimental procedure and electrolyte composition, and they do not have a rigorous urea quantification procedure. It requires a thorough reinvestigation to get clear insights. Since then, there have been various investigations in this field utilizing different approaches and methodologies to further understand urea synthesis³³⁻³⁷ from NO₃- and CO₂, as well as from NO₂- and CO³⁸. Feng et al.³⁹ reports a 12.2 % urea Faradaic efficiency (FE) at -1.1 V vs. RHE from the electrochemical reduction of NO₂ and CO₂ on Te-doped Pd nanocrystal. Leverett et al.⁴⁰ used a single-atom Cu catalyst for the electrochemical reduction of NO₃- and CO₂ to urea with 28 % urea FE at -0.9 V vs. RHE. Meng et al.41 synthesized ZnO porous nanosheets for electrosynthesis of urea from NO₂⁻ and CO₂ with a urea FE of 23.26 % at -0.79 V vs. RHE. Lv et al.⁴² report a very high urea FE of 53.4 % from the electrochemical reduction of NO₃⁻ and CO₂ on In(OH)₃ based catalyst⁴³. A detailed summary of the urea FE and current density obtained on prominent catalysts reported in the literature is given in the supporting information (Table S1). A thorough catalyst screening to selectively synthesize urea is not available in the existing literature. In an alkaline medium, the cathodic, anodic, and overall reactions are:

Cathode:
$$2 \text{ NO}_3^- + \text{CO}_2 + 11 \text{H}_2\text{O} + 16 e^- \rightarrow \text{NH}_2\text{CONH}_2 + 18 \text{OH}^ E^0 = 0.78 \text{ V vs. RHE}$$

Anode: $16 \text{OH}^- \rightarrow 4 \text{O}_2 + 8 \text{H}_2\text{O} + 16 e^ E^0 = 1.23 \text{ V vs. RHE}$
Overall: $2 \text{NO}_3^- + \text{CO}_2 + 3 \text{H}_2\text{O} \rightarrow \text{NH}_2\text{CONH}_2 + 4 \text{O}_2 + 2 \text{OH}^ E^0 = 0.45 \text{ V vs. RHE}$

In this work, we report a near ~100% selectivity for urea from the electrochemical reduction of NO_3^- and CO_2 on Ag catalysts. The rest of article is organized as follows: A detailed experimental catalyst screening is performed on the prominent catalysts; electrochemical urea synthesis is performed on Ag catalyst by varying the applied potential, and a mechanism is proposed; the effect of the concentrations of NO_3^- and CO_2 on the urea FE and urea current density are studied; the stability of the Ag is assessed by performing an electrochemical urea synthesis reaction (USR) for a period of 9 h; Ag is characterized using XRD and XPS pre and post-electrolysis followed by operando FTIR studies; and DFT calculations are done to understand the reaction pathways for

urea formation on Ag catalysts. This work aims to overcome the challenges in urea production by establishing an electrocatalytic system that utilizes a wide range of CO₂ and nitrate feedstocks to produce urea in a single, sustainable, and more energy-efficient process as shown in Figure S24.

Methods

All the details regarding the materials and chemicals used, such as manufacturer, part number, and purity, are given in the supporting information (Table S2 and S3).

Electrochemical Experiments

All the electrochemical urea synthesis experiments were conducted in a custom 3D-printed flow cell (Figure S3). Pt was used as the counter electrode, Ag/AgCl/sat. KCl was used as the reference electrode and 25 % HNO $_3$ was used as the anolyte. The catholyte and anolyte were separated by using Nafion 117 membrane. Nafion 117 membrane was pre-treated by soaking it in 3 % H_2O_2 at 80 °C for 1 h, followed by deionized (DI) H_2O at 80 °C for 2 h, and followed by 0.5 M H_2SO_4 at 80 °C for 1 h. The membrane is rinsed between each step using DI H_2O and the final treated membrane is stored in the DI H_2O . The anolyte volume used was 5 ml and it was kept stationary in the anolyte side. The catholyte volume used was 30 ml and it flowed from a reservoir to the catholyte side using a peristaltic pump at a rate of 40 ml/min. The electrodes were polished before experiments for 10 mins using a finer polishing pad (*Pike Technologies – Crystal Polishing Kit #162-400*) by using a ceria-based polishing compound (*Pike Technologies – Polishing Compound #162-4014*) followed by sonicating the electrodes in DI water for 10 mins after which they are dried in Ar.

For the catalyst screening, the effect of applied potential, and stability studies, a catholyte solution of 0.1 M KNO₃ and 0.1 M KHCO₃ was used. For the effect of concentration of NO₃⁻, the following solution concentrations were used: 1 M KNO₃ + 0.1 M KHCO₃, 0.5 M KNO₃ + 0.1 M KHCO₃, 0.1 M KNO₃ + 0.1 M KHCO₃, 0.1 M KNO₃ + 0.1 M KHCO₃, and 0.001 M KNO₃ + 0.1 M KHCO₃. The solution was sparged with CO₂ by using a sparger for 15 mins such that the solution was equilibrated with CO₂. The pH of the solution was measured before and after electrolysis by using a pH probe. Gas products were collected during the experiment using a gas bag by flowing Ar at a rate of 30 sccm for a period of 30 mins. Liquid products remain in the catholyte, and hence, the catholyte was collected in a vial post-electrolysis. The possible gas products are CO, CH₄, H₂, and N₂. The gas products were quantified using gas chromatography (GC) (*SRI Multiple Gas Analyzer*). The possible liquid products are NH₃, urea, NO₂⁻, and HCOOH. NH₃ and urea were quantified by using colorimetric techniques, NO₂⁻ was quantified by using lon exchange chromatography (IC) (*Metrohm*), and the rest of the products were quantified by using high-performance liquid chromatography (HPLC) (*Agilent 1200 HPLC*).

The electrolysis was carried out for a period of 1h by using a potentiostat (*Biologic SP 300*). Potentio-electrochemical impedance spectroscopy (PEIS) was performed before all the experiments to measure the electrolyte resistance between the Luggin capillary of the reference electrode and the surface of the cathode. PEIS was performed by setting a single sine wave mode

scanned from frequencies 100 kHz to 30 Hz by measuring 10 points per decade, at an amplitude of 20 mA with 3 measures per frequency, and the scan was repeated once. The working electrode voltage was set to 0 V vs open circuit, the voltage range was set to -10 V to 10 V and the current range was set to Auto. 85 % of uncompensated IR drop was compensated through positive feedback using the Biologic EC-Lab software. 15 % of uncompensated IR drop was compensated manually during the calculations. LSV was performed at a scan rate of 5 mV/s from 0 to -3 V vs. RHE, with an acquisition time of 0.05 s. The voltage range was set to -10 V to 10 V and the current range was set to Auto. CA was performed with an acquisition time of 0.1 s, with a voltage range of -10 V to 10 V and the current range was set to 1 A. For the stability studies, similar settings were used that of CA but with an acquisition time

Electrochemical 48-hour stability tests

The use of 25% HNO3 in our 9-hour test was intended to reduce the overpotential in the anodic chamber. We hypothesize that a pH difference between the chambers could cause substantial variation, potentially affecting long-term product stability. Therefore, for the 48-hour stability experiment, we used the same electrolyte in both the anolyte and catholyte chambers to maintain consistent conditions and ensure reliable results. A **Glass H-cell** (Pike Technologies) was used to conduct the 48-hour stability experiment. The cell was equipped with a **silver planar electrode** as the working electrode, with **copper tape** serving as the current collector. The electrolyte solution, consisting of **0.1 M KNO₃** and **0.1 M KHCO₃**, was used as both the catholyte and anolyte. The two chambers of the H-cell were separated by an **Excellion membrane**. The experiment was conducted at ambient temperature, with a **platinum electrode** serving as the counter electrode. An **Ag/AgCl reference electrode** was placed in the catholyte solution.

Colorimetric quantification of products

NH₃ was quantified by the Indophenol blue method⁴⁴. To 1 ml of the electrolyte sample, 1 ml of KOH solution, 500 μ L of phenol nitroprusside solution and 500 μ L of sodium hypochlorite solution are added and the resulting solution was incubated in the dark for half an hour. The sample changes color from colorless to blue. The sample was scanned for absorbance as a function of wavelengths from 400 to 800 nm using a visible spectrometer (*Genesys 30 Visible Spectrometer*). The maximum absorbance was observed at 632 nm and hence 632 nm was chosen to measure absorbances and quantify NH₃. Calibration graphs (Absorbances vs. concentration of NH₃) were prepared for different concentrations of NH₃ in the electrolyte. Separate calibration graphs were prepared when the concentration of the electrolyte was changed, as the absorbances were sensitive to the pH of the solution. The NH₃ calibration graphs for different electrolyte compositions are provided in Figure S4 of the supporting information.

Urea was quantified by the Diacetylmonoxime method⁴⁵. To 1 ml of the electrolyte sample, 1 ml of acid-ferric solution and 2 ml of monoxime-carbazide solution are added. The resulting sample

is heated at 100 °C with constant stirring for 5 mins followed by cooling at room temperature for 5 mins. The sample changes color from colorless to pink. The sample was scanned for absorbance as a function of wavelengths from 400 to 800 nm using a visible spectrometer. The maximum absorbance was observed at 525 nm, and hence, 525 nm was chosen to measure the absorbances and quantify urea. Calibration graphs (Absorbances vs. concentration of urea) were prepared for different concentrations of urea in the electrolyte. Separate calibration graphs were prepared when the concentration of the electrolyte was changed for improved accuracy, as it was observed that the absorbances were sensitive to the electrolyte solution. The urea calibration graphs for different electrolyte compositions are provided in Figure S5 of the supporting information. In the presence of NH₃, formamide, methyl amine, and acetamide, the diacetylmonoxime method does urea not provide а color change, and it is selective for (Figure S10).

Possible sources of error in colorimetric quantification of products:

The colorimetric quantification of urea using the diacetyl monoxime (DAMO) method is prone to several sources of error, including human and experimental errors. Matrix effects, such as the presence of complex electrolytes or high salt concentrations, can influence absorbance measurements through light scattering or interference with the chromogenic reaction, leading to inaccuracies. Additionally, small timing differences between absorbance measurements of the same solution can introduce variability.

To minimize these errors, we conducted each urea synthesis experiment in triplicate. After each electrochemical reaction, the post-electrolyte solution was collected, and the urea concentration was measured three times to account for any variability in absorbance readings. Recognizing the sensitivity of electrochemical experiments, each experiment was repeated three times to address potential errors arising from electrochemical factors. Furthermore, whenever the salt concentrations were altered, new calibration curves were generated to account for matrix effects and ensure accurate quantification.

One source of error we observed is the pH change in the post-electrolyte after an hour of reaction, which occurs due to the generation of OH⁻ ions. This results in an increase in pH, which can affect the colorimetric method and lead to slight errors in urea quantification, potentially causing overestimation. The pH change can also alter absorbance measurements, which may affect Faradaic efficiency (FE) calculations.

Supplementary Figures S4, F2, and E2 highlight this effect. Specifically, Figures F2 and H2 compare 0.1M KNO₃ + 1M KHCO₃ with 0.1M KNO₃ + 0.01M KHCO₃. As shown in these graphs, the slopes and intercepts differ significantly when bicarbonate concentrations change, which in turn affects the pH and absorbance. While we have addressed most potential sources of error, this pH shift remains a contributing factor to the observed overestimation of FE.

NMR quantification

For the 1 H NMR tests, dimethylsulfoxide-d6(DMSO-d6) was adopted as deuterated reagents. First, 570 µL of extracted electrolyte without postprocessing was mixed well with 30 µL 10mM acetone prepared in DMSO-d6. Then, the liquid was transferred into the NMR tube for the test. The measurements are carried out on a Bruker 500 MHz AVANCE NEO spectrometer equipped with a cryoprobe. The presented data is the accumulated result of 64 scans. The water resonance was suppressed with the excitation sculpting method using a 3-ms 180° shaped pulse centered at 4.612 ppm. The perfect-echo variant was chosen to reduce J-modulation for the samples analyzed at 500 MHz. A total of 1,024 transient scans were recorded with an interscan delay of 1 s. 64,000 complex points were acquired for each free induction decay with an acquisition time of 3.4 s. The processed spectra were zero-filled to 64,000 real points, and an exponential apodization function with lb = 0.3 Hz was applied before Fourier transformation. DMSO (3 vol%; 99.9%, Sigma-Aldrich) was added for deuterium locking and referencing. The results are shown in Figure S15.

FE Calculation

Calibration curves for both NMR and UV-Vis techniques were generated and are provided in the Supplementary Information. These calibration plots were used to determine the concentration and moles of urea present in the post-reaction electrolyte samples.

To calculate the urea Faradaic efficiency (FE), the urea partial current density was first determined. The total moles of urea produced in the reaction were calculated from the calibration data. The partial current density for urea formation (in mA/cm²) was then calculated using

the

following

equation:

Urea Current Density
$$\left(\frac{\text{mA}}{cm^2}\right) = \frac{\text{Moles of urea} \times n \times F \times 1000}{t}$$

where:

- n is the number of electrons transferred during urea formation (16 electrons for urea, 6 electrons for ammonia),
- F is Faraday's constant (96,485 C/mol),
- t is the reaction time in seconds.

The total urea current density was then divided by the total applied current density to calculate the Faradaic efficiency:

FE (%) =
$$\frac{\textit{Urea current density} \times 100\%}{\textit{Total current density}}$$

This method accounts for the total charge passed in the electrochemical reaction and allows for the calculation of urea FE using both NMR and UV-Vis quantification techniques.

Catalyst Characterization

XPS was performed using *Kratos Axis-165* to analyze the surface composition and the oxidation states of the Ag catalyst before and after electrolysis. Our samples required minimal preparation; specifically, we only attached them to the holder using carbon tape. We conducted surface analysis for the Ag planar electrode and AgGDE, without performing depth profiling. Calibration was achieved using the carbon peak in the XPS, with a pass energy of approximately 200 eV and a pressure below 10^{-8} mbar. Carbon tape was used for electrical contact. The instrument produced monochromatized Al K α radiation at 12 kV and 10 mA. A survey scan was conducted between binding energies 0 and 900 eV with a resolution of 1 eV. Following the survey scan, high-resolution scans were conducted between 560 and 620 eV to identify the Ag 3p peaks, between 360 and 380 eV to identify the Ag 3d peaks, and between 520 and 540 eV to identify the O 1s peak with a resolution of 0.1 eV. To minimize the noise, 5 sweeps were performed for the high-resolution scans.

XRD was performed on the Ag electrode before and after electrolysis using *Bruker D8 Discover X-ray Diffractometer* using Cu K α radiation (λ = 1.5418 Å) generated at 40 kV and 40 mA. K β coming from Cu radiation was filtered by using Ni filters. The diffractometer has parallel beam optics and a 0.5° parallel slit analyzer. On the primary side, Göbel mirror was used and on the detector side LYNXEYE detector, which has 196 channels, each having a channel width of 14.4 mm was used. The detector slit used was 1.2 mm. A two-theta scan was performed to get the offset of the beam with the sample holder in place by using a primary rotary absorbance value of 73.88 following which an external offset correction was made. The sample was placed on the sample holder, and a Z scan was performed to locate the sample edge with an auto primary rotary absorbance. The angular offset of the sample was found by performing a rocking scan with a primary rotary absorbance of 73.88, and flatness correction was made. Finally, two theta/theta scans were coupled from 10° to 90° with a step size of 0.02° to obtain the XRD spectra. The primary rotary absorbance was set to auto mode. Post-processing was performed using Diffrac Suite Eva software, and the background noise was subtracted. The data were scanned with the ICDD and the peaks were identified.

FTIR experiments were conducted similar to previously established studies on nitrate reduction mechanisms.²⁵ The experiments were performed on a *Bruker Invenio-S infrared spectrometer*. A custom-made electrochemical cell was mounted on top of a 60⁰-face angled Ge crystal was setup on a ATR VeeMax-III variable angle accessory (*Pike Tech.*). To enhance the metal wettability of the Ge crystal and the conductivity of the substrate, an IR transparent indium-tin-oxide (ITO) layer of 100 nm was sputter coated over it, using an *EMS Quorum 150TS plus* sputter coater. Silver (Ag) was sputter coated on top of this ITO layer with a thickness of 2 nm. After subtracting

the background of the base electrolyte, a potential of -0.1 vs RHE was applied and the spectra were acquired at different time stamps with a resolution of 2 cm $^{-1}$ averaged over 10 scans. A liquid N $_2$ -cooled mid-band mercury cadmium telluride (MCT) detector was used while conducting these measurements. The schematic of the setup used is provided in the supporting information (Figure S6). For ex-situ experiments, we use a ZnSe crystal mounted on a heating plate for our analysis. The temperature is set at 110 °C to evaporate all the water, and solid residues will be crystallized on the ZnSe crystal, which is then used for analysis in Attenuated total reflectance (ATR) mode.

Xenemetrix Ex-Calibur EX-2600 was used for **XRF** analysis. This instrument uses a Rh X-ray source, operated here at 20 keV and 10 μ A, and a silicon energy-dispersive detector. For the analysis, 200 μ L of the solution was deposited onto a piece of filter paper and allowed to dry. Once completely dried, the filter paper was placed into the XRF instrument for analysis. A qualitative survey scan was performed using a standard XRF instrument with a rhodium (Rh) source. The 20 versus intensity data and the software-generated peak list were analyzed.

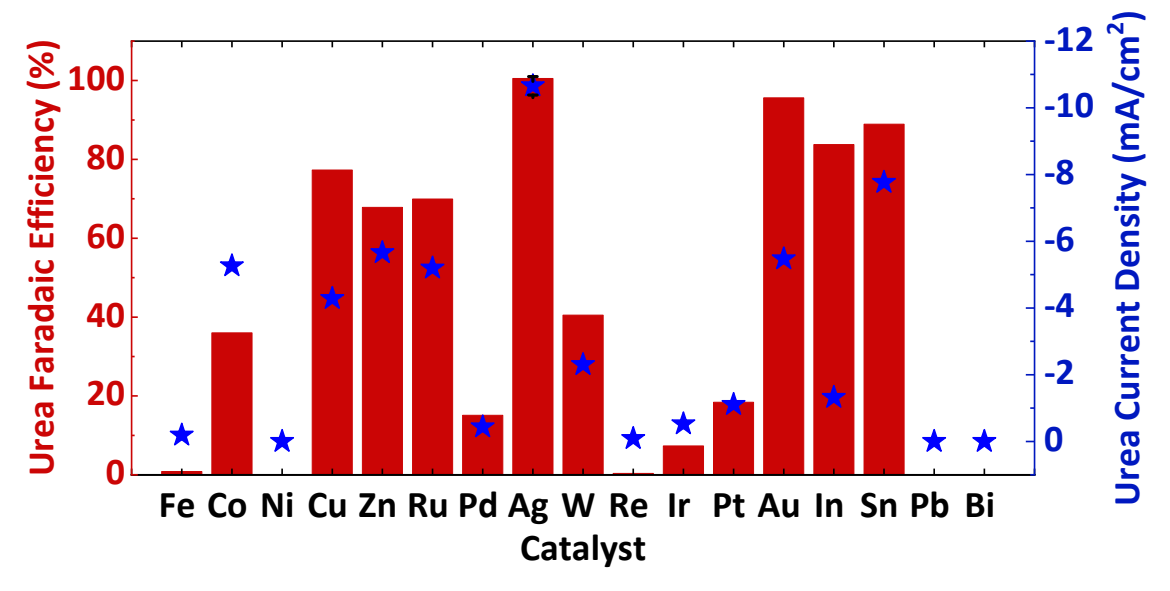
DFT Methods

All density functional theory (DFT) calculations were performed using the Vienna Ab initio Simulation Package (VASP)⁴⁶⁻⁴⁸ interfaced with the Atomic Simulation Environment (ASE)⁴⁹. DFT calculations in conjunction with the computational hydrogen electrode (CHE) model⁵⁰ were used to determine intermediate adsorption energies of the urea and formamide formation pathways. Core electrons were described using PAW pseudopotentials⁵¹, and valence electrons were expanded as planewaves up to a kinetic energy cutoff of 500 eV. The electron exchange and correlation interactions were accounted for using the revised Perdew-Burke-Ernzerhof (RPBE) exchange-correlation functional by Hammer and Nørskov⁵². Solvation effects were incorporated using a continuum solvation model as implemented in VASP (VASPsol)^{53, 54}. A (3 × 3 × 1) Monkhorst-Pack⁵⁵ k-point mesh was used to sample the Brillouin zone. Adsorbate binding energies were calculated using a 3 x 3 x 3 supercell with the bottom two layers fixed and the top layer free to relax with the adsorbate. Geometries were considered to be optimized after the maximum force on each unconstrained atom fell below 0.05 eV/Å. The transition states for the two C-N bond formation reactions were estimated using a constrained one-dimensional bondlength scan at constant potential as described and benchmarked in our previous publications^{56,} ⁵⁷. Briefly, the bond length is varied over a series of 25 images spanning the initial state (e.g. *CO + *NO) to the final state (e.g. *CONO). At each image, the C-N bond length is constrained, and the geometry is optimized at constant potential with respect to this constraint. The adsorptionfree energies, ΔG of the reaction intermediates are calculated using the expression ($\Delta G_{ads} = \Delta E_{ads}$ + Δ ZPE – T Δ S), where Δ E is the difference in electronic energy of the adsorbed species, Δ ZPE is the difference in zero-point energies, and ΔS is the change in entropy of the adsorbed species with respect to the catalyst surface.⁵⁸ The ZPE and entropies S were calculated using the Harmonic Oscillator approximation, which assumes that adsorbed molecules vibrate harmonically and have only vibrational degrees of freedom. The reaction mechanisms for the various elementary steps and further details of the simulation cell can be found in the supplementary material (Figures S5 and S6). The highest energy image was then refined to a true transition state using the improved Dimer method as implemented in VASP Transition State Tools.^{59, 60}

Results and Discussions Catalysts Screening

Different metallic catalysts are screened for the electrochemical synthesis of urea from NO₃⁻ and CO₂. The Electrochemical reaction is performed in a custom-made flow cell where the solution of 0.1 M KNO₃ and 0.1 M KHCO₃ equilibrated with CO₂ is used as the catholyte. Chronoamperometry is performed by applying a constant potential of -1 V vs. RHE for a period of 1h. A detailed experimental procedure is given in the methods section. In total, 17 different catalysts are chosen for the study, including the prominent electrochemical CO₂ reduction catalysts⁶¹ such as Cu, Zn, Ag, Au, Sn, In, Re, and Pb, and catalysts active for electrochemical NO₃⁻ reduction⁶² to NH₃ such as Co, Ni, Fe, and Pd. The catholyte is tested for urea and NH₃ post-electrolysis using colorimetric methods. A detailed procedure on the quantification methods for urea and NH₃ is provided in the methods section. The catalyst that exhibits the highest urea Faradaic efficiency (FE) and the highest urea current density (CD) is preferred.

Figure



1 denotes the urea FE and urea CD for different catalysts. Bi and Re do not show any activity for urea. Pt and Ir show minimal activity for urea synthesis. Pt, Ir, and Re are good hydrogen evolution reaction (HER) catalysts.⁶³ The activity of Pt towards HER is significantly suppressed in the presence of nitrates. For Re and Ir, the suppression of HER activity is less than that of Pt. Catalysts

that exhibit good activity for electrochemical NO_3^- reduction to NH_3 such as Fe, Ni, and Pd show very less activity for urea. NH_3 is observed in significant amounts for these catalysts. Co is the best catalyst for electrochemical NO_3^- reduction to NH_3^{25} and it is also active for electrochemical CO_2 reduction to CO and $HCOOH.^{64}$ Co shows a good urea CD (~-5mA/cm²) but the urea FE is less (~30%) and NH_3 is the dominant product when Co is used. Cu that is active for both electrochemical CO_2 reduction and electrochemical NO_3^- reduction to NH_3 shows good activity for urea with 70 % urea FE, but the urea current density (~-4 mA/cm²) is lesser than that of Co.

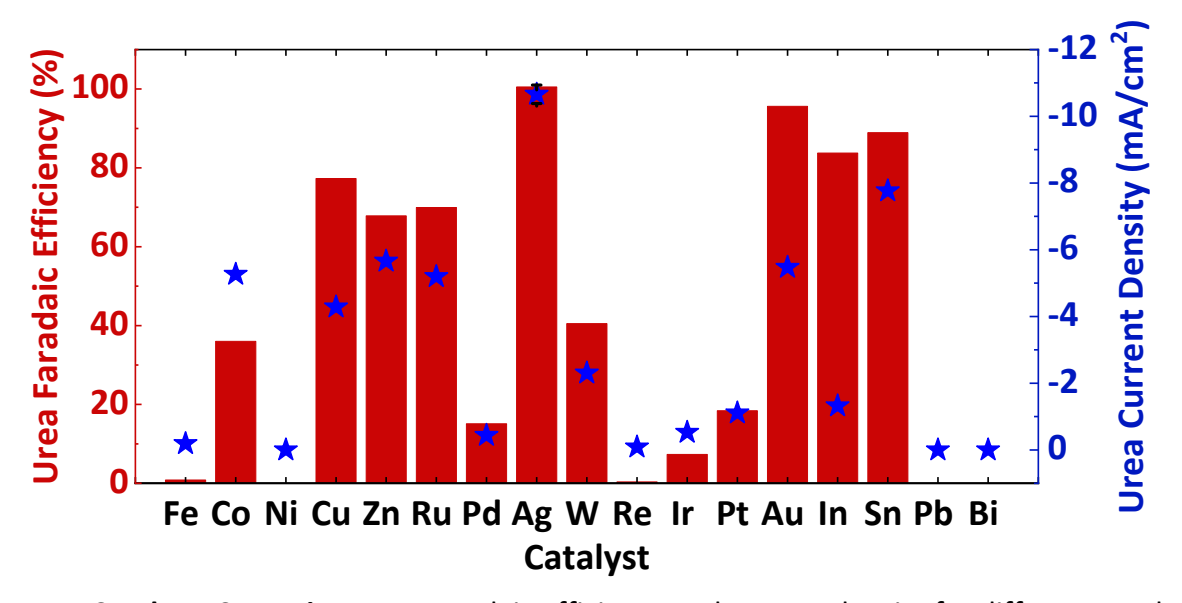


Figure 1: Catalysts Screening Urea Faradaic efficiency and current density for different catalysts at -1 V vs. RHE.

In, Zn, and Sn are active for electrochemical CO₂ reduction to HCOOH and CO, and they show higher urea FEs (>80 % for In and Sn, and >60 % for Zn). Ag and Au (prominent catalysts for electrochemical CO₂ reduction to CO) show enhanced activities for urea synthesis with >95 % urea FEs, and Ag exhibits the highest urea current density (~-8 mA/cm²) and ~100 % urea FE. Pb, which is the most active catalyst for electrochemical CO₂ to HCOOH, shows no activity towards urea. We hypothesize that the reaction intermediates for CO formation are also key intermediates for urea synthesis. Also, Pb does not show activity toward electrochemical CO formation, and this strengthens our hypothesis. We believe that In, Sn, and Zn, which are active for urea synthesis, primarily facilitate CO₂ reduction with HCOOH as the dominant product. In contrast, Ag and Au, which also show activity for urea, mainly produce CO during CO₂ reduction. The CO₂ reduction mechanisms differ between these two groups, leading us to hypothesize that C-N coupling may also proceed via distinct mechanisms. From the above study, we observe that Ag exhibits the highest urea FE and urea CD, and hence Ag is chosen for further evaluations to improve the catalytic activity and understand the urea formation mechanism. Understanding the mechanism of urea formation on catalysts that reduce CO₂ to HCOOH is beyond the scope of this study and is a potential future work.

Electrochemical Measurements

Figure 2A denotes the linear sweep voltammetry (LSV) profiles for different catholyte solutions when Ag is used as the cathode. Three electrolyte solutions are considered for the study, namely 0.1 M KHCO₃, 0.1 M KNO₃, and 0.1 M KHCO₃ + 0.1 M KNO₃. The first and the last solutions are equilibrated with CO₂ before the study, whereas 0.1 M KNO₃ is not equilibrated with CO₂. A detailed description of the potentiostat settings used to perform LSV and other experiments in this section is given in the methods section. The possible Faradaic reactions when 0.1 M KHCO₃ is used as the electrolyte are the CO₂ reduction reaction (CO₂RR) to CO and HER, NO₃ reduction reaction (NORR) to NO₂-, NH₃, and N₂ when 0.1 M KNO₃ is used as the electrolyte and urea synthesis reaction (USR) along with HER, CO₂RR to CO and NORR when a solution of 0.1 M KHCO₃ and 0.1 M KNO₃ is used as the electrolyte. The slope of the LSV profile gets steeper when the solution of 0.1 M KHCO₃ and 0.1 M KNO₃ is used in comparison to individual electrolyte solutions indicating possible USR. The experimentally measured onset potential for the NORR when 0.1 M KNO₃ is used is 0.04 V and for the CO₂RR when 0.1 M KHCO₃ is used is -0.42 V. For the solution containing both 0.1 M KHCO₃ and 0.1 M KNO₃, the onset potential is measured to be -0.22 V. A zoomed-in figure denoting the onset potentials is provided in the supporting information (Figure S1).

The effect of applied potential on the electrochemical USR is studied to understand the potential dependence on the selectivity of urea. A solution of 0.1 M KNO₃ and 0.1 M KHCO₃ equilibrated with CO₂ is chosen as the electrolyte, and the applied potential is varied from -0.6 to -1.5 V vs. RHE. Figure 2B denotes the urea FE and urea current density as a function of the applied potential. As the applied potential is increased in the negative direction, the urea CD increases linearly. For all the applied potentials, the urea FE remains close to 100 %. This indicates that the Ag catalyst is very selective for the electrochemical USR for the electrolyte concentration of 0.1 M KNO₃ and 0.1 M KHCO₃. The selectivities of electrochemical CO₂RR products such as CO, CH₃OH, and C₂H₄ are potentially driven and the selectivities drop drastically when the applied potential is changed by even 0.2 V vs. RHE due to the competing HER.¹⁷ It has been reported in the literature that the HER is drastically suppressed even in the presence of small amounts of NOx.⁶⁵ The presence of concentrated amounts of nitrates in our system suppresses the HER and hence the urea selectivity remains constant (~100%) in the studied potential range. At higher overpotentials (electrochemical urea synthesis), the urea FE drops significantly, and NH₃ FE increases due to over reduction of NO₃. The urea and NH₃ performance at high overpotentials is provided in Figure S2 of the supporting information.

The effect of the concentration of NO_3^- on the selectivity of urea is investigated. The concentration of bicarbonates is kept constant in the electrolyte (0.1 M KHCO₃) and the concentration of NO_3^- (1, 0.5, 0.1, 0.01, and 0.001 M KNO₃) is varied. For all the above cases, the electrolyte is equilibrated with CO_2 , and chronoamperometry is performed at -1 V vs. RHE. **Figure 2C** denotes the FEs of the products and urea current densities as the concentration of NO_3^- is changed by fixing the concentration of bicarbonate. As the concentration of NO_3^- is increased,

the urea current density increases as a function of the concentration of NO_3^- . At lower concentrations of NO_3^- , CO is observed to a great extent. As the concentration of NO_3^- is increased NH_3 is observed along with decreasing concentration of CO, indicating that NORR is more preferred than CO_2RR . Beyond 0.1 M of NO_3^- , only urea is observed, and other by-products such as CO, H_2 , and NH_3 are not observed. This indicates that the concentration of NO_3^- is a key parameter in deciding the selectivity of urea apart from the applied potential.

The stability of the Ag towards electrochemical USR is studied for a period of 9 h by performing chronoamperometry at -1 V vs. RHE by using a solution of 0.1 M KNO₃ and 0.1 M KHCO₃ equilibrated with CO₂ as the catholyte. The products are sampled every 1h and Figure 2D denotes the urea FE and urea CD as a function of time. A constant urea FE of ~100 % is observed, and the urea CD remains constant throughout the study period, indicating that Ag is stable for the electrochemical USR. Additionally, we performed a long-term stability test with a 48-hour experiment. Given the extended duration, we replaced the analyte with the same electrolyte used in the catholyte (0.1M KNO₃ + 0.1M KHCO₃), instead of HNO₃, to prevent the migration of H⁺ from the anolyte over time. The performance remained consistent, with the system continuously producing urea at a Faradaic efficiency of nearly 90% as shown in Figure S18. So far, all the analyses are performed on planar Ag. To improve the urea CD, 10 nm of Ag was sputter coated on a carbon paper, which acts as a gas diffusion electrode (GDE), and the reaction was carried out by using 1 M KNO₃ and 0.1 M KHCO₃ equilibrated with CO₂. The urea CD improved drastically in comparison with planar Ag, although an order of magnitude improvement is not observed as the NO3- is still in the liquid phase, and only the CO2 concentration is improved in the gas phase. Figure 2E denotes the effect of applied potential when Ag-GDE is used as the electrode. At -1.25 V vs. RHE, ~100 % urea FE and ~-100 mA/cm² urea current density is observed and this is the highest so far reported in literature.

The urea quantification results obtained through UV-Vis analysis were validated using ¹H NMR. The ¹H NMR spectrum of the post-electrolysis sample displayed a peak at a chemical shift of 5.5 ppm, corresponding to urea, with a Faradaic efficiency (FE) estimated to be approximately 98%. To benchmark the NMR technique against UV-Vis spectrometry, a parity plot was generated, showing a slope close to 1, indicating a strong correlation between the two methods (as illustrated in Figure S15D). Additionally, to confirm that the urea originates from nitrate rather than contamination, isotope-labeled nitrate (¹⁵KNO₃) was used in the electrolyte for urea synthesis with an Ag planar electrode, yielding an FE of 88%. The isotope peaks in the ¹H NMR spectrum appear at 5.17 ppm and 5.47 ppm, with a coupling constant of 180 Hz, further validating the formation of urea in our electrochemical setup. Detailed NMR spectra and calibration graphs are provided in the supplementary information. We have also performed an extended stability test for a period of 48 hours, as shown in Figure S18.

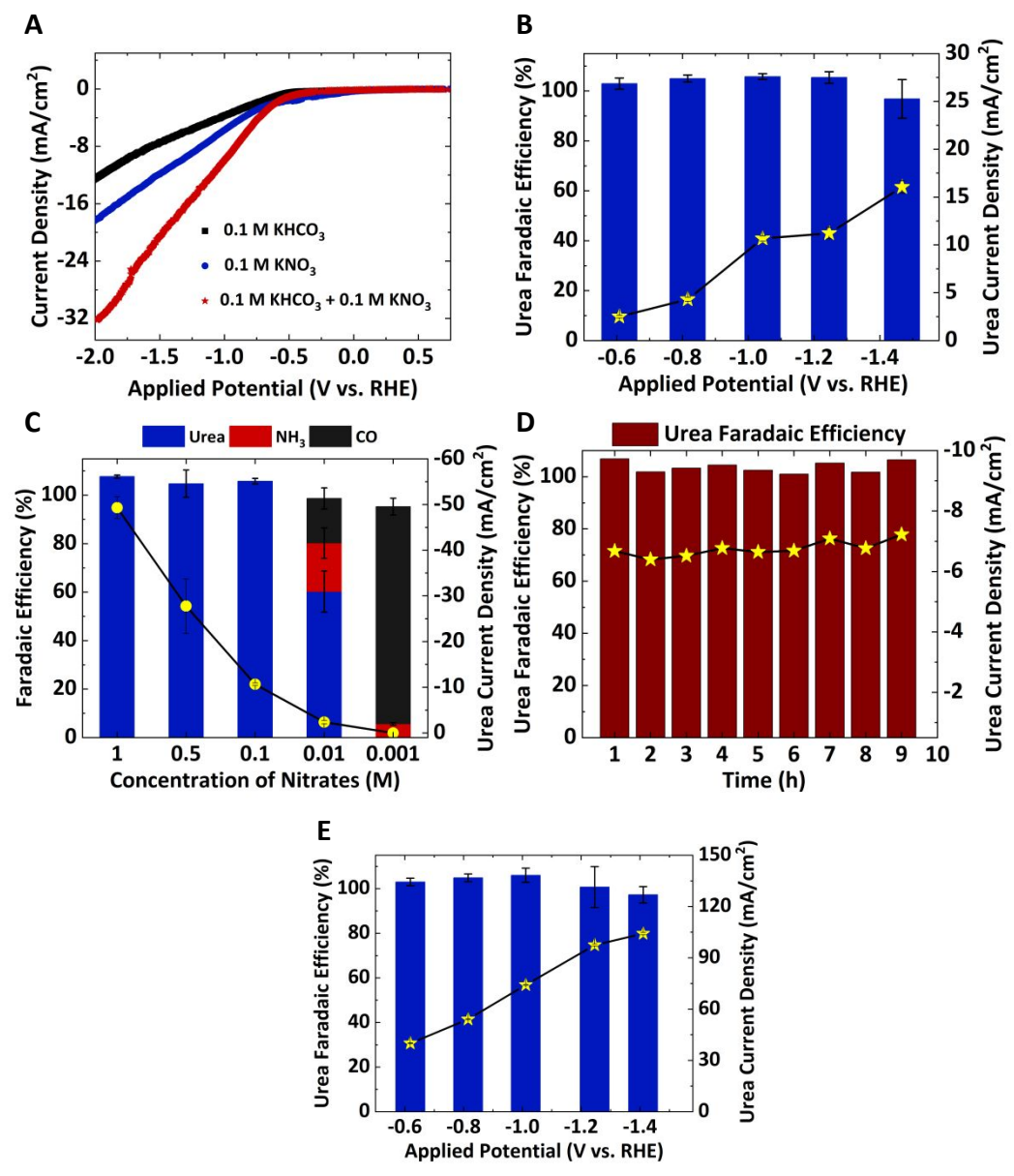


Figure 2: Electrochemical Measurements: All experiments are performed at room temperature with 1cm^2 electrode area. In all the cells the flowrate of electrolyte was maintained at 30 ml/min. A) Linear sweep voltammetry (LSV) profiles for Ag cathode using different catholytes such as 0.1 M KHCO₃ (equilibrated with CO₂), 0.1 M KNO₃ and a solution of 0.1 M KHCO₃ and 0.1 M KNO₃ (equilibrated with CO₂). B) Urea Faradaic efficiency and current density as a function of applied potential using Ag cathode and by using a solution of 0.1 M KNO₃ and 0.1 M KHCO₃ equilibrated with CO₂ as the catholyte for run time of 1 hour. (Yellow symbols indicate urea current density in all the figures) C) Urea, NH₃, and CO Faradaic efficiencies and urea current density as a function of the concentration of NO₃- after 1-hour electrochemical experiment. The solution contains 0.1 M KHCO₃ and the concentration of NO₃- is varied as 1, 0.5, 0.1, 0.01, and 0.001 M respectively which is equilibrated with CO₂. D) Urea Faradaic efficiency and current density as a function of time showing the stability of Ag for electrochemical urea synthesis. The solution was not

constantly sparged with CO_2 . E) Urea Faradaic efficiency and current density as a function of applied potential using Ag GDE and by using a solution of 1 M KNO₃ and 0.1 M KHCO₃ equilibrated with CO_2 as the catholyte, with experimental run time of 30 mins.

Catalyst Characterization

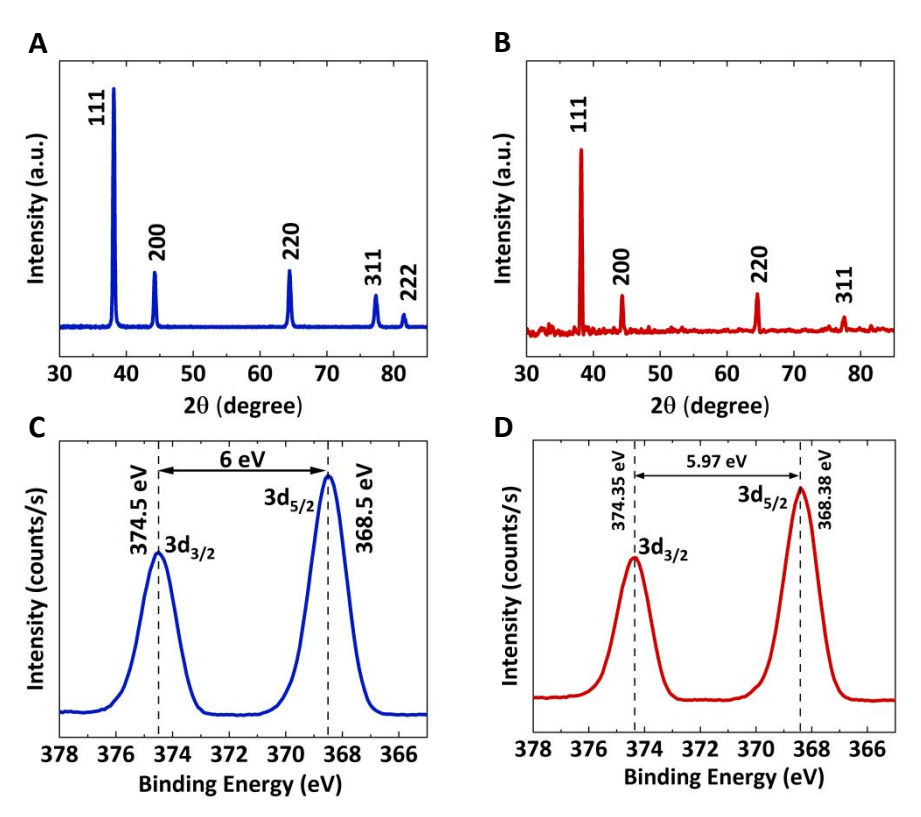


Figure 3: Catalyst Characterization X-ray diffraction (XRD) spectra of planar Ag, A) Preelectrolysis, and B) Post-electrolysis. X-ray photoelectron spectra (XPS) for planar Ag, C) Preelectrolysis, and D) Post-electrolysis.

X-ray diffraction (XRD) spectroscopy and X-ray photoelectron spectroscopy (XPS) ⁶⁶are performed on Ag catalyst pre and post-electrolysis to understand the facets present on the Ag and its oxidation states. A detailed description of the experimental methods used to perform XRD and XPS is given in the methods section.

Figure 3A denotes the XRD spectra for Ag catalyst pre-electrolysis. Peaks are observed at 20 locations corresponding to 38.11°, 44.23°, 64.42°, 77.32°, and 81.55°. The spectra match identically with metallic Ag as per the International Centre for Diffraction Data (ICDD No. 04-0783). 111 is the prominent facet observed on the Ag used for electrochemical USR. **Figure 3B** denotes the XRD spectra for the Ag catalyst post-electrolysis. A slight noise is observed in the data, but the peaks corresponding to the 20 locations match with the metallic Ag, indicating that the facets are preserved, and there is no structural reorganization of the catalyst post-reaction.

Figure 3C denotes the spectra obtained from XPS performed on Ag pre-electrolysis. Two prominent peaks are observed at binding energies corresponding to 374. 5 and 368.5 eV. These peak locations correspond to Ag $3d_{3/2}$ and Ag $3d_{5/2}$. The location of Ag $3d_{5/2}$ at 368.5 eV and the difference in binding energies between Ag 3d_{5/2} and Ag 3d_{5/2} (6 eV) indicate that Ag is in its metallic state.⁶⁷ Negligible shift (~0.12 eV) in the Ag 3d_{5/2} binding energy peak is observed for the Ag post electrolysis denoted by Figure 3D, and the catalyst still remains in its metallic state, indicating that there is no change in the oxidation state of the catalyst after performing 1 h of electrochemical USR. No significant change is observed on Ag GDE before and after electrolysis Scanning Electron Microscopy (SEM) images (Figure XRF analysis was performed to determine if Ag leaching occurred during extended periods of cell operation, as shown in Figure S23. The results indicated that most observed peaks were

attributed to the Rh source and the sample holder, including prominent Rh-K α and Rh-K β lines. However, no silver (Ag) peaks were identified in the qualitative survey scan, despite the analysis specifically targeting Ag detection. This suggests that no Ag leaching occurred under the reductive conditions in the electrolyte during the 48-hour stability test. Following the characterization of the Ag planar electrode, the Ag gas diffusion electrode (AgGDE) was also analyzed using XPS. As illustrated in Figures S26 and S27, the silver in AgGDE remains in its metallic state after electrolysis. Additionally, Auger spectra for both pre-and post-electrolysis were collected, revealing the presence of AgM4N45N45 and AgM5N45N45 in both conditions, as shown in Figure S28⁶⁶.

In-situ FTIR Studies

Electrochemical co-reduction of CO₂ and NO₃ are performed on Ag electrode at -1 V vs. RHE, and operando attenuated total reflectance surface-enhanced infrared absorption spectra are obtained as a function of time. 0.1 M KNO₃ & 0.1 M KHCO₃ equilibrated with CO₂ is used as the electrolyte. Background subtraction was performed using the blank electrolyte before acquiring the FTIR spectra. The details of the experimental procedure are provided in the methods section. Several peaks appeared corresponding to different functional groups, and **Figure 4**A denotes the obtained FTIR spectra. The peaks are identified by the FTIR database and from the Sadler Handbook of infrared spectra. Further ex-situ experiments were conducted on the reactants and products to analyze better and identify the peaks. (Figures S7 denote the FTIR spectra of reactants and products). Further details on the obtained spectra are provided in the supporting information section.

The prominent peak appears at peak location corresponding to 1487 cm⁻¹ in the C-N stretching region as shown in **Figure 4**B. As there is no significant rise in peak intensities in C-H stretching region, we could rule out the possibilities of methyl amine and formamide. Hence, the C-N stretching peak could be attributed to urea formation. There is a rise in the intensity of the C=O stretching bands corresponding to urea between wavenumbers 1500 and 1750 cm⁻¹ as shown **Figure 4**C in Both of these signatures indicate the formation of urea. The *CO adsorption peak is observed in in-situ FTIR analysis at around ~1942 cm⁻¹ during the electrochemical urea synthesis reaction as shown in **Figure 4**D. A similar observation is reported in the literature.² The intensity of the peak rises as a function of time and drops down denoting that CO is a key intermediate for the electrochemical urea synthesis reaction. The intensity of the peaks between wavenumbers 3500 and 3100 cm⁻¹ increases as a function of time. This corresponds to the N-H stretching of urea as shown in **Figure 4**E.

The in-situ electrochemical analysis provides strong evidence for the formation of urea (in addition to the colorimetric results), and CO* intermediates are observed. The in-situ data is consistent with the DFT calculations performed for urea formation on the Ag electrode, which is discussed in the following section.

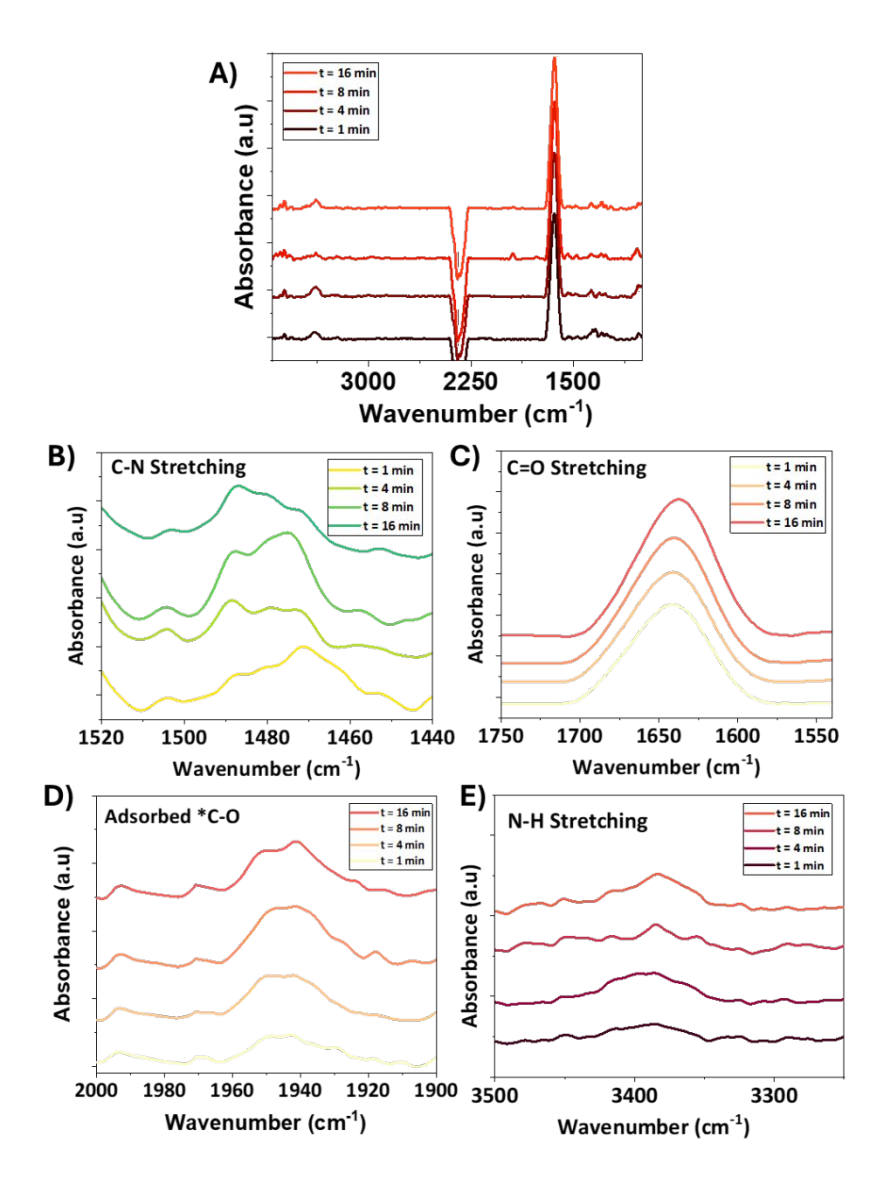


Figure 4: Attenuated total reflectance surface-enhanced infrared absorption spectra (ATR-SEIRAS) A) In-situ FTIR spectra obtained using ATR-SEIRAS for the electrochemical co-reduction of NO_3^- and CO_2 on planar Ag at -1 V vs. RHE at 1 min, 4 min, 8 min, and 16 min. B) C-N Stretching at 1487 cm⁻¹. C) C=O stretching at 1640 cm⁻¹. D) C-O stretching at 1942 cm⁻¹. E) N-H stretching at 3384 cm⁻¹.

DFT Investigation of Electrocatalytic C-N Coupling

DFT calculations are performed to investigate the pathways toward the electrochemical synthesis of urea and formamide on Ag (100), (111), and (110), beginning with the two reacting

species (CO_2 and NO_3^-). A schematic of one feasible proposed pathway on low-index facets of Ag is given in **Figure 5**.

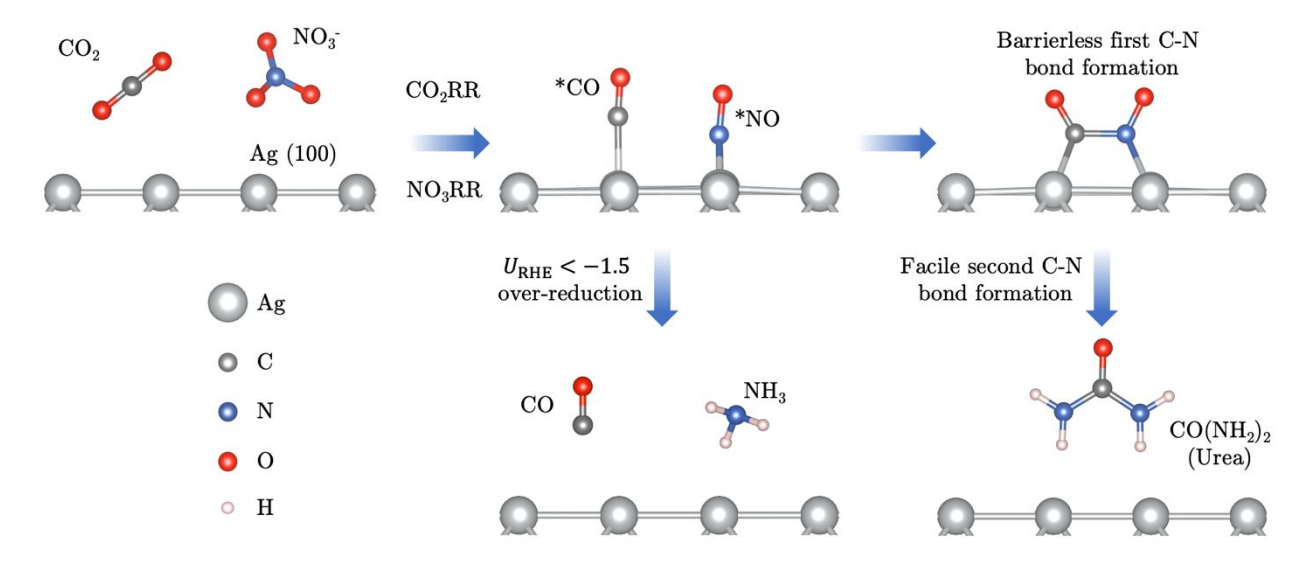


Figure 5: One of several feasible pathways for the electrochemical synthesis of urea via the coreduction of CO_2 and NO_3 over a Ag catalyst.

To arrive at this proposed pathway, we calculated the free energy of adsorption of each species at potentials between 0 V and -1.5 V vs. RHE, as shown in **Figure 6A**. As in previous works^{19, 25}, adsorption of NO_3^- anions are considered via the reaction given in Eq. 1:

$$NO_{3}^{-}(aq) + H_{2}O + e^{-} + * \rightarrow * NO_{2} + 2OH^{-}$$
 (1)

We remark here that the initial adsorption of nitrate is poorly understood; the reaction $NO_3^-+*\to *NO_3+e^-$ is an *oxidation* reaction that will be unfavorable under reducing conditions. One may also consider the reductive adsorption of nitric acid, HNO₃. Given the dissociation equilibrium coefficient for nitric acid ($^{\circ}0.4 \text{ eV}$)^{19, 68}, the availability of this species is likely vanishingly small ($^{\circ}1$ in $^{\circ}10^{\circ}1$

$$CO_2(g) + H_2O + e^- + * \rightarrow *COOH + OH^-$$
 (2)

The reaction free energy is calculated to be positive ($\approx +1.26$ eV) at 0 V vs. RHE, indicating that CO₂ adsorption is unfavorable at moderately reducing potentials, consistent with reports from previous studies suggesting that CO₂ adsorption is rate-limiting during electrochemical CO₂ reduction on Ag^{70,71}. On Ag(100) the free energy of the coupled CO₂ and protonation will be more

favorable as the potential becomes more reducing, becoming spontaneous at -1.26 V vs. RHE based on the computational hydrogen electrode model. This value coincides with experimental reports at -1.25 V vs. RHE, at which ~100 % urea FE and ~-100 mA/cm² urea current density was observed. We note that CO_2 adsorption will occur at less reducing potentials on more reactive, high index facets, possibly explaining experimental observation of urea current at less reducing potentials. Also, as shown in Eq. 3, a concerted coupled proton-electron transfer step followed by an Eley-Rideal like C-N bond coupling step can also occur between adsorbed nitrogen species (*NO) and CO_2 to produce *NOCOOH. The reaction free energy for this step is calculated to be +0.37 eV at 0V vs RHE, becoming spontaneous at -0.37 V vs. RHE on Ag(100). This value is closer to -0.22 V vs RHE, which is the experimentally observed on-set potential for urea synthesis

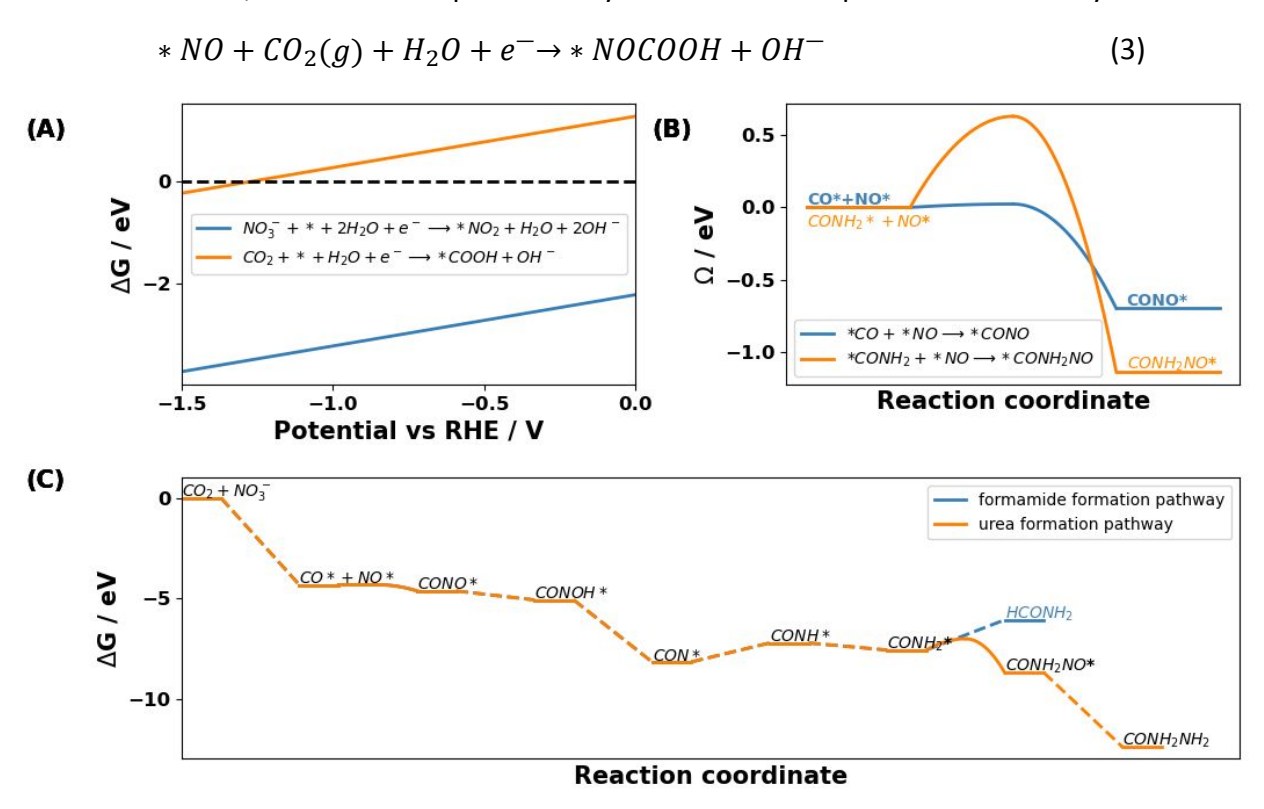


Figure 6: DFT Results (A) Adsorption energy of NO_3^- and CO_2 (B) C-N bond formation barrier on Ag(100) (C) Free energy diagram for CO_2 and Nitrate co-reduction at OV vs. RHE

Based on our prior analysis finding that NO_3^- reduction on weaker nitrogen binding catalysts (such as Ag) is limited by the protonation of *NO to form *NOH²⁵ and that the main product of CO_2 reduction on Ag is $CO^{70,72}$, we propose that the first C-N bond formation for the co-reduction of NO_3^- and CO_2 will occur between adsorbed CO and NO (*CO + *NO \rightarrow *CONO). As shown in **Figure 6B**, DFT is used to calculate the first C-N bond formation barrier on Ag at constant potential (see methods section for further details). Barrier calculations for coupling reactions of NO with CO_2 , *COOH, and *CO on other low-index facets of Ag are given in the SI. We report a barrierless

coupling of *CO and *NO on Ag (100), and very low barriers on other low-index facets of Ag. Coupling of *NO with *COOH similarly exhibits very low barriers, effectively instantaneous on the timescale of a reaction turnover, suggesting that the dominant coupling mechanism will be driven by the steady-state availability of reactants, rather than being limited by an activation barrier. In the absence of a full microkinetic model of the process, it is not possible to conclusively comment on the predominant mechanism of the first C-N bond formation step, only that it occurs without a significant activation barrier. Given prior reports of *CO being the predominant surface species for CO_2 reduction on Ag, 72,73 in addition to our previously published analysis of nitrate reduction on transition metals, 74 we hypothesize that the coupling mechanism *CO and *NO may be the predominant pathway for the first C-N bond formation step.

To probe the reaction pathway beyond the first C-N bond formation step, all possible reaction pathways are investigated, and the free energy of the various intermediates is calculated (see Figure S8 and S9 in the SI for further details) under reaction conditions with the free energy diagram for the most thermodynamically favorable pathway shown in **Figure 6C.**

Our calculations reveal that the second C-N bond formation may occur after a series of protonation steps (*CONH₂ + *NO \rightarrow *CONH₂NO, Δ G < 0). We find that additional protonation of adsorbed *CONH₂ to produce HCONH₂ (formamide) is thermodynamically unfavorable (Δ G > 1.5 eV at 0 V vs. RHE), consistent with the lack of formamide detected by experimental efforts. The second C-N bond formation barrier for this reaction on Ag (100) is also calculated. Our results suggest that the second C-N bond formation barrier, which we found to be 0.56eV - 0.62 eV, is likely not rate determining given the reported current density towards urea. The free energy diagram, shown at 0V vs. RHE, illustrates that the energies of all the elementary steps in this reaction are exergonic except for the protonation of adsorbed CON (*CON + H⁺ + e⁻ \rightarrow *CONH). However, as this step is a reduction step, it becomes more favorable at a more cathodic potential. From our DFT results, we hypothesize that urea synthesis from the co-reduction of CO₂ and nitrate on Ag is limited by either i) CO₂ adsorption on the catalyst surface, or ii) mass transport of reactants from the bulk electrolyte to the reaction plane. The urea current density is drastically improved when GDE configuration is used, which supports this hypothesis.

Summary and Conclusions

Electrochemical C-N coupling to synthesize urea from NO_3^- and CO_2 is not thoroughly investigated in the literature, and in this work, we performed a thorough catalyst screening and reported that Ag is selective, active, and stable for the electrochemical synthesis of urea. CO_2 transport to the Ag surface and adsorption are limiting factors as in the case of electrochemical CO_2RR . It is demonstrated that GDE configuration overcomes the limitation and a very high urea current density of ~-100 mA/cm² and a urea Faradaic efficiency of ~100 % is observed at -1.25 V vs. RHE. which is the highest so far reported in the literature. The concentration of NO_3^- plays a key role in the selectivity, and a minimum concentration of 0.1 M KNO₃ is required for ~100 % selectivity, and at lower concentrations of $NO_3^ CO_2RR$ becomes dominant instead of USR. Our DFT calculations reveal that on Ag (100), a combination of facile first and second C-N bond formation

steps and an endergonic formamide formation step from *CONH₂ results in its improved kinetics and selectivity towards urea synthesis. We believe that the current work would potentially lead to further studies on the electrochemical C-N coupling for high value-added chemicals.

Acknowledgments

This material is based on the work performed in the Materials and Systems Engineering Laboratory at the University of Illinois Chicago (UIC) and Gauthier's Lab at Texas Tech University in collaboration with Glusac's Lab (UIC). M.R.S. acknowledges funding from UIC.

Conflict of Interest

Authors declare no conflict of interest.

Author Contributions

N.C.K. and I.G. prepared and characterized the catalysts under the direction of M.R.S. The electrocatalytic experiments were performed by N.C.K. and I.G. guided by M.R.S. The analysis of liquid products was performed by N.C.K. and I.G., guided by M.R.S. NMR experiments were performed by S.C. under the guidance of K.G. FTIR was performed by R.R.B. under the supervision of M.R.S. Theoretical calculations were performed by S.O., directed by J.A.G. The manuscript was composed by N.C.K., I.G., S.O., R.R.B., J.A.G., and M.R.S. M.R.S. devised the project, conceptualized the main ideas, and worked on almost all the technical aspects.

Additional Information

Supplementary information The online version contains supplementary material available at .

Correspondence and requests for materials should be addressed to Meenesh R. Singh or Joseph A. Gauthier.

References

- 1. P. M. Glibert, J. Harrison, C. Heil and S. Seitzinger, *Biogeochemistry*, 2006, **77**, 441-463.
- 2. D. Milani, A. Kiani, N. Haque, S. Giddey and P. Feron, *Sustainable Chemistry for Climate Action*, 2022, 100008.
- 3. A. H. Conner, *Polymeric materials encyclopedia*, 1996, **11**.
- 4. S. Dammalapati, P. Aghalayam and N. Kaisare, *Industrial & Engineering Chemistry Research*, 2019, **58**, 20247-20258.
- 5. N. Balaji, P. Aghalayam and N. S. Kaisare, *Industrial & Engineering Chemistry Research*, 2018, **57**, 6853-6862.
- 6. B. Carl and M. Wilhelm, *Journal*, 1922.
- L. Wang, M. Xia, H. Wang, K. Huang, C. Qian, C. T. Maravelias and G. A. Ozin, *Joule*, 2018, 2, 1055-1074.
- 8. S. Giddey, S. Badwal, C. Munnings and M. Dolan, *ACS Sustainable Chemistry & Engineering*, 2017, **5**, 10231-10239.

- 9. G.-F. Chen, Y. Yuan, H. Jiang, S.-Y. Ren, L.-X. Ding, L. Ma, T. Wu, J. Lu and H. Wang, *Nature Energy*, 2020, **5**, 605-613.
- 10. N. C. Kani, A. Prajapati, B. A. Collins, J. D. Goodpaster and M. R. Singh, *ACS Catalysis*, 2020, **10**, 14592-14603.
- 11. N. C. Kani, A. Prajapati and M. R. Singh, ACS ES&T Engineering, 2022, 2, 1080-1087.
- 12. N. C. Kani, N. H. L. Nguyen, K. Markel, R. R. Bhawnani, B. Shindel, K. Sharma, S. Kim, V. P. Dravid, V. Berry and J. A. Gauthier, *Advanced Energy Materials*, 2023, **13**, 2204236.
- 13. L. Barrera and R. Bala Chandran, *ACS Sustainable Chemistry & Engineering*, 2021, **9**, 3688-3701.
- 14. M. Xia, C. Mao, A. Gu, A. A. Tountas, C. Qiu, T. E. Wood, Y. F. Li, U. Ulmer, Y. Xu and C. J. Viasus, *Angewandte Chemie International Edition*, 2022, **61**, e202110158.
- 15. J. M. McEnaney, S. J. Blair, A. C. Nielander, J. A. Schwalbe, D. M. Koshy, M. Cargnello and T. F. Jaramillo, *ACS Sustainable Chemistry & Engineering*, 2020, **8**, 2672-2681.
- 16. S. Nitopi, E. Bertheussen, S. B. Scott, X. Liu, A. K. Engstfeld, S. Horch, B. Seger, I. E. Stephens, K. Chan and C. Hahn, *Chemical reviews*, 2019, **119**, 7610-7672.
- 17. A. Prajapati, N. C. Kani, J. A. Gauthier, R. Sartape, J. Xie, I. Bessa, M. T. Galante, S. L. Leung, M. H. Andrade and R. T. Somich, *Cell Reports Physical Science*, 2022, **3**, 101053.
- 18. E. L. Clark, S. Ringe, M. Tang, A. Walton, C. Hahn, T. F. Jaramillo, K. Chan and A. T. Bell, *ACS catalysis*, 2019, **9**, 4006-4014.
- 19. J.-X. Liu, D. Richards, N. Singh and B. R. Goldsmith, ACS Catalysis, 2019, 9, 7052-7064.
- 20. B. Qin, Y. Li, H. Fu, H. Wang, S. Chen, Z. Liu and F. Peng, *ACS applied materials & interfaces*, 2018, **10**, 20530-20539.
- 21. Y. Wang, W. Zhou, R. Jia, Y. Yu and B. Zhang, *Angewandte Chemie International Edition*, 2020, **59**, 5350-5354.
- 22. L. Barrera, R. Silcox, K. Giammalvo, E. Brower, E. Isip and R. Bala Chandran, *ACS Catalysis*, 2023, **13**, 4178-4192.
- 23. J. Lim, C.-Y. Liu, J. Park, Y.-H. Liu, T. P. Senftle, S. W. Lee and M. C. Hatzell, *ACS Catalysis*, 2021, **11**, 7568-7577.
- 24. P. Li, Z. Jin, Z. Fang and G. Yu, *Energy & Environmental Science*, 2021, **14**, 3522-3531.
- 25. N. C. Kani, J. A. Gauthier, A. Prajapati, J. Edgington, I. Bordawekar, W. Shields, M. Shields, L. C. Seitz, A. R. Singh and M. R. Singh, *Energy & Environmental Science*, 2021.
- 26. X. Deng, Y. Yang, L. Wang, X. Z. Fu and J. L. Luo, *Advanced Science*, 2021, **8**, 2004523.
- 27. S. Han, H. Li, T. Li, F. Chen, R. Yang, Y. Yu and B. Zhang, *Nature Catalysis*, 2023, **6**, 402-414
- 28. M. Shibata and N. Furuya, *Electrochimica acta*, 2003, **48**, 3953-3958.
- 29. M. Shibata, K. Yoshida and N. Furuya, *Journal of the Electrochemical Society*, 1998, **145**, 2348.
- 30. M. Shibata, K. Yoshida and N. Furuya, *Journal of the Electrochemical Society*, 1998, **145**, 595.
- 31. M. Shibata and N. Furuya, *Journal of Electroanalytical Chemistry*, 2001, **507**, 177-184.
- 32. M. Shibata, K. Yoshida and N. Furuya, *Journal of Electroanalytical Chemistry*, 1998, **442**, 67-72.
- 33. Y. Luo, K. Xie, P. Ou, C. Lavallais, T. Peng, Z. Chen, Z. Zhang, N. Wang, X.-Y. Li, I. Grigioni, B. Liu, D. Sinton, J. B. Dunn and E. H. Sargent, *Nature Catalysis*, 2023, **6**, 939-948.

- 34. X. Huang, Y. Li, S. Xie, Q. Zhao, B. Zhang, Z. Zhang, H. Sheng and J. Zhao, *Angewandte Chemie International Edition*, **n/a**, e202403980.
- 35. J. Geng, S. Ji, M. Jin, C. Zhang, M. Xu, G. Wang, C. Liang and H. Zhang, *Angewandte Chemie International Edition*, 2023, **62**, e202210958.
- 36. M. Jiang, M. Zhu, M. Wang, Y. He, X. Luo, C. Wu, L. Zhang and Z. Jin, *ACS Nano*, 2023, **17**, 3209-3224.
- 37. Y. Zhao, Y. Ding, W. Li, C. Liu, Y. Li, Z. Zhao, Y. Shan, F. Li, L. Sun and F. Li, *Nature Communications*, 2023, **14**, 4491.
- 38. H. Wan, X. Wang, L. Tan, M. Filippi, P. Strasser, J. Rossmeisl and A. Bagger, *ACS Catalysis*, 2023, **13**, 1926-1933.
- 39. Y. Feng, H. Yang, Y. Zhang, X. Huang, L. Li, T. Cheng and Q. Shao, *Nano Letters*, 2020, **20**, 8282-8289.
- 40. J. Leverett, T. Tran-Phu, J. A. Yuwono, P. Kumar, C. Kim, Q. Zhai, C. Han, J. Qu, J. Cairney and A. N. Simonov, *Advanced Energy Materials*, 2022, **12**, 2201500.
- 41. N. Meng, Y. Huang, Y. Liu, Y. Yu and B. Zhang, *Cell Reports Physical Science*, 2021, **2**, 100378.
- 42. C. Lv, L. Zhong, H. Liu, Z. Fang, C. Yan, M. Chen, Y. Kong, C. Lee, D. Liu and S. Li, *Nature Sustainability*, 2021, **4**, 868-876.
- 43. L. Zhengyi, Z. Peng, Z. Min, J. Hao, L. Hu, L. Shengqi, Z. Heng, Y. Song and Z. Zehui, *Applied Catalysis B: Environmental*, 2023, **338**, 122962.
- 44. S. Z. Andersen, V. Čolić, S. Yang, J. A. Schwalbe, A. C. Nielander, J. M. McEnaney, K. Enemark-Rasmussen, J. G. Baker, A. R. Singh and B. A. Rohr, *Nature*, 2019, **570**, 504-508.
- 45. C. Chen, X. Zhu, X. Wen, Y. Zhou, L. Zhou, H. Li, L. Tao, Q. Li, S. Du and T. Liu, *Nature chemistry*, 2020, **12**, 717-724.
- 46. G. Kresse and J. Furthmüller, *Physical review B*, 1996, **54**, 11169.
- 47. G. Kresse and J. Furthmüller, Computational materials science, 1996, 6, 15-50.
- 48. G. Kresse and J. Hafner, *Physical review B*, 1993, **47**, 558.
- 49. A. H. Larsen, J. J. Mortensen, J. Blomqvist, I. E. Castelli, R. Christensen, M. Dułak, J. Friis, M. N. Groves, B. Hammer and C. Hargus, *Journal of Physics: Condensed Matter*, 2017, **29**, 273002.
- 50. J. K. Nørskov, J. Rossmeisl, A. Logadottir, L. Lindqvist, J. R. Kitchin, T. Bligaard and H. Jonsson, *The Journal of Physical Chemistry B*, 2004, **108**, 17886-17892.
- 51. G. Kresse and D. Joubert, *Physical review b*, 1999, **59**, 1758.
- 52. B. Hammer, L. B. Hansen and J. K. Nørskov, *Physical review B*, 1999, **59**, 7413.
- 53. K. Mathew, R. Sundararaman, K. Letchworth-Weaver, T. Arias and R. G. Hennig, *The Journal of chemical physics*, 2014, **140**, 084106.
- 54. K. Mathew, V. C. Kolluru, S. Mula, S. N. Steinmann and R. G. Hennig, *The Journal of Chemical Physics*, 2019, **151**, 234101.
- 55. H. J. Monkhorst and J. D. Pack, *Physical review B*, 1976, **13**, 5188.
- 56. J. A. Gauthier, Z. Lin, M. Head-Gordon and A. T. Bell, *ACS Energy Letters*, 2022, **7**, 1679-1686.
- 57. J. A. Gauthier, J. H. Stenlid, F. Abild-Pedersen, M. Head-Gordon and A. T. Bell, *ACS Energy Letters*, 2021, **6**, 3252-3260.

- 58. J. A. Zamora Zeledón, M. B. Stevens, G. K. K. Gunasooriya, A. Gallo, A. T. Landers, M. E. Kreider, C. Hahn, J. K. Nørskov and T. F. Jaramillo, *Nature Communications*, 2021, **12**, 620.
- 59. A. Heyden, A. T. Bell and F. J. Keil, *The Journal of chemical physics*, 2005, **123**.
- 60. G. Henkelman and H. Jónsson, *The Journal of Chemical Physics*, 1999, **111**, 7010-7022.
- 61. Y. i. Hori, *Modern aspects of electrochemistry*, 2008, 89-189.
- 62. X. Fu, J. Zhang and Y. Kang, *Chem Catalysis*, 2022.
- 63. J. Greeley, T. F. Jaramillo, J. Bonde, I. Chorkendorff and J. K. Nørskov, *Nature materials*, 2006, **5**, 909-913.
- 64. M. Usman, M. Humayun, M. D. Garba, L. Ullah, Z. Zeb, A. Helal, M. H. Suliman, B. Y. Alfaifi, N. Iqbal and M. Abdinejad, *Nanomaterials*, 2021, **11**, 2029.
- 65. B. H. Ko, B. Hasa, H. Shin, E. Jeng, S. Overa, W. Chen and F. Jiao, *Nature communications*, 2020, **11**, 1-9.
- 66. A. M. Ferraria, A. P. Carapeto and A. M. Botelho do Rego, *Vacuum*, 2012, **86**, 1988-1991.
- 67. K. D. Bomben, J. F. Moulder, P. E. Sobol and W. F. Stickle, *Perkin-Elmer Corporation*, 1992.
- 68. F. Calle-Vallejo, M. Huang, J. B. Henry, M. T. Koper and A. S. Bandarenka, *Physical chemistry chemical physics*, 2013, **15**, 3196-3202.
- 69. H.-C. Mi, C. Yi, M.-R. Gao, M. Yu, S. Liu and J.-L. Luo, *ACS Applied Materials & Interfaces*, 2022, **14**, 43257-43264.
- 70. J. Hussain, H. Jónsson and E. Skúlason, *Acs Catalysis*, 2018, **8**, 5240-5249.
- 71. W. Deng, P. Zhang, B. Seger and J. Gong, *Nature Communications*, 2022, **13**, 803.
- 72. M. R. Singh, J. D. Goodpaster, A. Z. Weber, M. Head-Gordon and A. T. Bell, *Proceedings of the National Academy of Sciences*, 2017, **114**, E8812-E8821.
- 73. J. Hussain, H. Jonsson and E. Skúlason, ACS Catalysis, 2018, 8, 5240-5249.
- 74. N. C. Kani, J. A. Gauthier, A. Prajapati, J. Edgington, I. Bordawekar, W. Shields, M. Shields, L. C. Seitz, A. R. Singh and M. R. Singh, *Energy & Environmental Science*, 2021, **14**, 6349-6359.

The data supporting this article have been included as part of the Supplementary Information.